Journal of Magnetic Resonance 214 (2012) 302–308

Contents lists available at SciVerse ScienceDirect

Journal of Magnetic Resonance

journal homepage: www.elsevier.com/locate/jmr

A compact high-speed mechanical sample shuttle for field-dependent high-resolution solution NMR

Ching-Yu Chou [a,b], Minglee Chu [c], Chi-Fon Chang [d], Tai-huang Huang [a,b,d,*]

[a] Department of Physics, National Taiwan Normal University, Taipei 116, Taiwan, ROC
[b] Institute of Biomedical Sciences, Academia Sinica, Nankang, Taipei 115, Taiwan, ROC
[c] Institute of Physics, Academia Sinica, Nankang, Taipei 115, Taiwan, ROC
[d] Genomics Research Center, Academia Sinica, Nankang, Taipei 115, Taiwan, ROC

ARTICLE INFO

Article history:
Received 8 October 2011
Revised 16 November 2011
Available online 10 December 2011

Keywords:
Field-dependent NMR relaxation
High-speed sample shuttler
Field cycling
Nuclear magnetic relaxation dispersion (NMRD)
Servo-mechanical shuttler
Molecular dynamics

ABSTRACT

Analysis of NMR relaxation data has provided significant insight on molecular dynamic, leading to a more comprehensive understanding of macromolecular functions. However, traditional methodology allows relaxation measurements performed only at a few fixed high fields, thus severely restricting their potential for extracting more complete dynamic information. Here we report the design and performance of a compact high-speed servo-mechanical shuttle assembly adapted to a commercial 600 MHz high-field superconducting magnet. The assembly is capable of shuttling the sample in a regular NMR tube from the center of the magnet to the top (fringe field ~0.01 T) in 100 ms with no loss of sensitivity other than that due to intrinsic relaxation. The shuttle device can be installed by a single experienced user in 30 min. Excellent 2D-^{15}N-HSQC spectra of (u-^{13}C, ^{15}N)-ubiquitin with relaxation at low fields (3.77 T) and detection at 14.1 T were obtained to illustrate its utility in R_1 measurements of macromolecules at low fields. Field-dependent ^{13}C–R_1 data of (3,3,3-d)-alanine at various field strengths were determined and analyzed to assess CSA and ^{1}H–^{13}C dipolar contributions to the carboxyl ^{13}C–R_1.

1. Introduction

Ever since the discovery of NMR it was soon recognized that nuclear magnetic resonance relaxation contains rich information on molecular dynamics [1–7]. Indeed, the ability of NMR relaxation technique to provide macromolecular dynamics at atomic resolution has been well-documented and is unmatched by other techniques [8–13]. However, NMR relaxation measurements of macromolecules have almost always been conducted in a few fixed fields, even though it is well-known that field variation of the relaxation parameters contains much more complete dynamic information. It is time-consuming to conduct relaxation measurements at many magnetic fields, and measurements at lower field lack the high resolution and high sensitivity needed to resolve individual sites of complex and labile macromolecules.

In the past there have been several fruitful approaches to measure field-dependent NMR relaxation [14–19]. The nuclear magnetic relaxation dispersion (NMRD) method has provided interesting insight on water dynamics [20,21]. The switched-field method provided fast electronic switching of magnetic field up to ~2 T for probing dynamics on the millisecond time domain [18,19,22–24]. However, such a system is not suitable for probing site specific dynamics of large macromolecular systems due to limited chemical shift dispersion and poor sensitivity at low field. In the sample shuttling approach used previously the NMR sample is initially equilibrated at homogeneous high field. After the preparation period the sample is shuttled, as rapidly as possible, to a lower magnetic field during the relaxation period and back to high field for detection pneumatically [25]. The lower field is provided by a separate magnet in a dual magnet system [26,27], or using the stray field of the high-field magnet [25,28]. This approach retains the capability of resolution and sensitivity of a high-field, high resolution system and has been applied to investigate the dynamics of model membrane, nucleic acids, and proteins (for a review see [29]). However, it has the disadvantage of slower switching rate (>0.3 s). The strong mechanical impact during the pneumatic shuttling process can have a deleterious effect on the samples such as causing sample denaturation.

An important improvement is use of a stepper motor and timing belt system to move the entire probe in and out of the large NMR magnet, as demonstrated by Vieth and coworkers [30,31] and widely applied [32,33]. A recent variation of this idea is to move a sample alone in and out of the top of a commercial spectrometer that can be shared with conventional users. In this way the full capability of the commercial system can be used for preparation and readout. Recently, Redfield reported the design of such a highly

* Corresponding author at: Institute of Biomedical Sciences, Academia Sinica, Nankang, Taipei 115, Taiwan, ROC.
E-mail address: bmthh@ibms.sinica.edu.tw (T.-h. Huang).

1090-7807/$ - see front matter © 2011 Elsevier Inc. All rights reserved.
doi:10.1016/j.jmr.2011.12.001

reliable servo-mechanical system and briefly reviewed its capability and applications [29]. Here we report the design of a very compact mechanical field cycling shuttle system and demonstrate its utility for measuring ^{13}C- and ^{15}N-longitudinal relaxation of small amino acids and proteins. We incorporated a novel timing belt system to couple the shuttler to the servomotor for fast, accurate, and stable sample shuttling. The assembly can be readily adapted to any commercial spectrometer.

2. Experimental methods

2.1. General assembly of the shuttle device

The sample shuttling device was built to fit an existing Bruker AV600 spectrometer equipped with a 54 mm bore shielded magnet (Fig. 1). The system consists of the following components: A servomotor assembly consisting of a servomotor and a pulley/timing belt-drive; a rail inserted inside the center of the magnet for guiding the shuttle; a light-weight acrylic shuttle/sample assembly; and the control electronics. The electronics is interfaced to the spectrometer PC and the operation is triggered by the spectrometer pulse program. Rotation of the large pulley fixed on the motor shaft drives the timing belt to move in one direction, which then carries the shuttle/sample assembly up to the desired position. A second pulse at a predefined time point triggers the servomotor to run in the opposite direction, thereby returning the shuttle/sample assembly back to the center of the magnet. During shuttling only the motor/pulley/belt assembly and the shuttle/sample assembly are moving. Twelve optical sensors were attached at various points along the stationery rail for sensing the shuttle positions. The optical sensors are small LED/photo reflective optical switches which detect light reflected from the 2 mm wide white labels stuck on the shuttle surface and sample tube tip when passing through the sensors. After the system is installed on the magnet, only the servomotor assembly on top of the magnet is visible (Fig. 1A). The rail assembly is hidden inside the magnet (Fig. 1B). The design of each component is described in more details below:

2.2. The servomotor and power train assembly

The 750 W servomotor (model CSBL720, CSIM Inc., Taiwan) was mounted on a vertical plate (back plate) which was attached to a horizontal bottom plate fastened on top of the magnet (Fig. 2A). The servomotor was further supported by two L-shaped supports. The pulley/timing belt-drive consists of a large toothed pulley (pulley L in Fig. 1 and 120 mm OD × 10 mm thick made of MC nylon) tightly fixed on the shaft of the servomotor and a smaller toothed pulley with ceramic bearing (pulley S, 18 mm OD × 10 mm thick made of MC nylon) fixed at the 7th section of the rail (Fig. 1B and 2D). A timing belt (model T5; length, 250 cm; pitch, 5 mm; width, 6 mm. East Dragon precision Transmission Co., Taiwan) was mounted on the two pulleys to transfer the rotational motion of the servomotor to up–down translational motion for transporting the shuttle/sample assembly along the rail inside the magnet. There are two small freely rotating idler pulleys fixed on the upper part of the back plate to guide the belt to proper separation down the rail (Fig. 1B). A trough 8 mm wide × 8 mm deep on each interior side of the rail serves as housing for the timing belt (Fig. 2B). The servomotor assembly has dimensions 40 cm high × 20 cm wide × 13 cm deep.

2.3. The rail assembly

The U-shaped aluminum rail is 101 cm long and is assembled from eight precisely machined blocks (Fig. 2A). The top seven pieces have identical outside dimension 4.2 cm wide × 3 cm thick and have two partially-exposed guiding rods for guiding the shuttle movement (Fig. 2B). The two 11 mm × 3 mm troughs below these two rods are the belt housing. The inner base of the seventh block (Fig. 2D) was flattened so that the small pulley S can be installed coplanar with the timing belt. The 8th block (Fig. 2C) is a 4.2 cm thick aluminum centering flange with corners trimmed to fit the magnet bore snugly for properly positioning the rail in the magnet. The eight blocks are aligned precisely with two assembly rods and two guiding rods and screw-tightened at the ends. After assembled to the magnet the bottom of the centering flange has

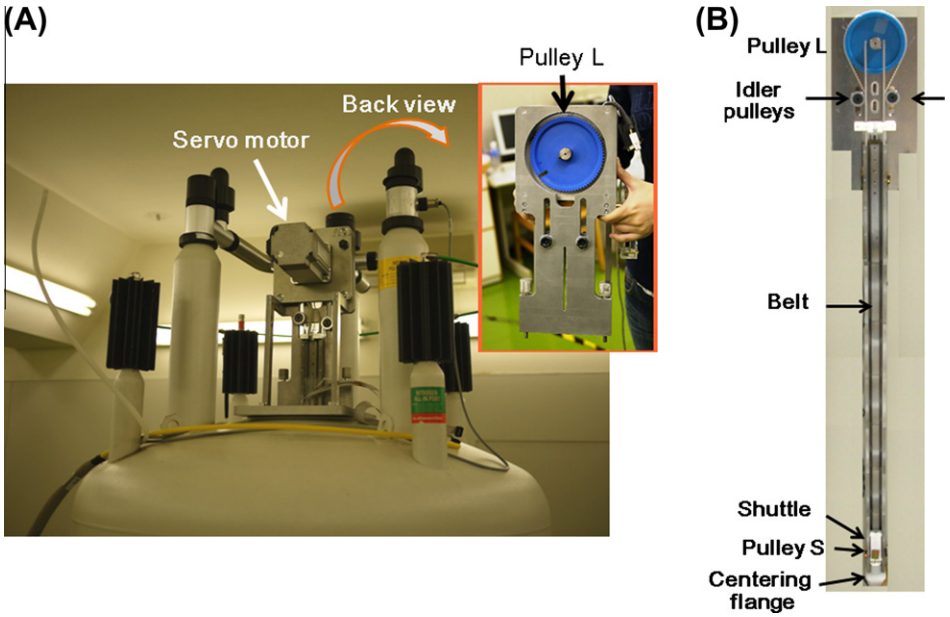

Fig. 1. Complete shuttle assembly. (A) Front view of the shuttle assembly after installed in the Bruker AV600 spectrometer. Only the upper part of the motor assembly is visible. The back view of the servomotor is shown as an insert. (B) Back view of the rail and pulley assembly outside the magnet. The large blue pulley L (OD 120 mm) is mounted on the shaft of the servomotor. The small pulley S (OD 18 mm) is mounted on the rail above the centering flange and is not visible from outside.

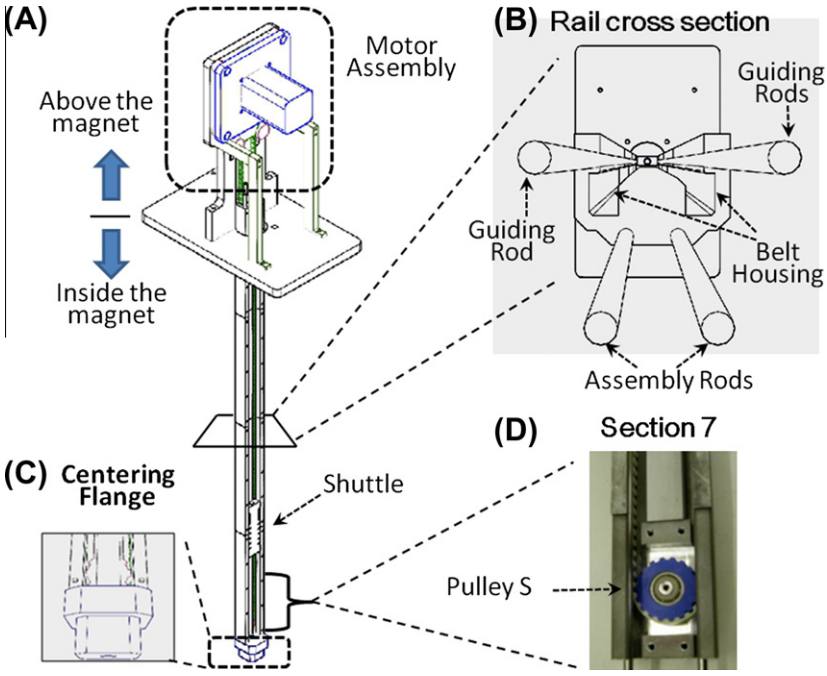

Fig. 2. (A) Schematics of the shuttle assembly. (B) The cross sectional view of the rail. (C) An expanded view of the centering flange at the bottom of the rail (8th piece of the rail). (D) Photograph of the 7th piece of the rail which has a flattened base to accommodate the small pulley S such that the pulley is coplanar with the timing belt. (For interpretation of color in figure, the reader is referred to the web version of this article.)

a 12 mm clearance above the probe. The top of the rail is attached to the vertical back plate and the timing belt is assembled afterward (Fig. 1B).

2.4. The shuttle and sample holder assembly

The rectangular acrylic shuttle (Fig. 3A) has a dimension of $8.6 \times 2.7 \times 1.1$ cm^3 and it weighs ~24 g (~35 g with the sample loaded). The middle 6.6 cm of the shuttle is 0.5 cm narrower on each side. A 1.0 cm × 0.5 cm × 0.5 cm trough was cut along the long axis at each corner for accommodating a 1.0 cm × 0.5 cm × 0.5 cm rectangular corner piece (material, sulfate-doped polyether ether ketone) (inset in Fig. 3A), which has a V-shaped groove in the middle and is screwed tightly to the shuttle (indicated by the arrows in Fig. 3A). The grooves are coplanar with the central axis of the magnet. They serve to position the shuttle between the two guiding rods precisely. These pieces are in contact with the guiding rods, thus are most likely to wear out. They can be replaced easily. To our surprise, there was no sign of wearing after 100,000 high-speed shuttling and no replacement of the corner piece was needed. A through-hole at the center of the shuttle parallel to the long axis serves as the housing for the sample-holder. The diameter of this hole is 8 mm for the upper 6.6 cm and narrowed to 7 mm for the remaining bottom 2 cm to restrict the downward movement of the sample holder.

The shuttle is coupled to one side of the timing belt through a 5 cm long F-shaped coupler (material: fiberglass reinforced plastics) which has a 10-teeth trough to clinch to the timing belt tightly (orange piece in Fig. 3). Thus, the shuttle can move up or down as the belt moves clockwise or counter clockwise. The pulleys and timing belt are positioned at 0.9 cm horizontal offset from the center axis of the magnet so as to place the sample housing in perfect center axis of the magnet. We note that Vieth's group is the first to use a timing belt to shuttle the sample but their design [30], as well as that of Redfield's [25], uses a stick coupled to the belt to move the shuttle and the complete moving assembly is heavier.

To ensure that the sample is firmly attached to the shuttle at all time during the shuttling process, and to minimize bubble formation, we have designed a sample holder assembly consisting of three pieces: a NMR tube holder, an insert, and a cap (Fig. 3B–D). The NMR tube holder (middle piece in Fig. 3B) is a 10.8 cm long polyether ether ketone (PEEK) tube of 5 mm inner diameter. The outer diameter of the holder is 8 mm for the upper 0.8 cm and narrowed to 7.5 mm for the lower part. The insert (Fig. 3C) is a 17 cm long rod. The diameter of the upper 16.6 cm is 4 mm with the top 5 cm threaded. The bottom 4 mm of the insert has a larger diameter of 4.2 mm which functions as a plug. The bottom of the plug has an inverted V-shaped indent (inset in Fig. 3C). A 1 mm diameter hole of 1 cm deep was drilled in the center of the plug. A small horizontal side hole was drilled at 1 cm above the lower end of the plug to connect to the center hole for excess sample to flow out to the tube chamber above the plug when inserted inside the regular 5 mm NMR tube (We used a Wilmad model 535-PP7 NMR tube). This arrangement allows convenient preparation of samples free of air bubbles in the sample chamber. The 1.5 cm long × 8 mm diameter screw nut (SN in Fig. 3C) is screwed on the threaded rod and can be moved up or down for proper positioning the tube insert with respect to the tube holder. The cap (top piece in Fig. 3B) is 4.3 cm long and 8 mm in outer diameter and it has a 4 mm hole (diameter) of 4.0 cm deep at the bottom. There is a 3 mm wide × 1 mm deep constriction groove in the middle of the cap (inset in Fig. 3B) for restricting the movement of the cap with respect to the shuttle by two screws (Fig. 3E). Fig. 3E shows the completely assembled shuttle/sample assembly.

2.5. The electronic control board

The control electronics consists of the motor driver module, the optical sensor circuitry and the digital control circuitry. The motor driver module is provided by the manufacturer and is interfaced to the PC through a RS232 port for uploading firmware programs. The interface communication program is written in Visual Basic and stored in the spectrometer PC. Both the motor drive module and

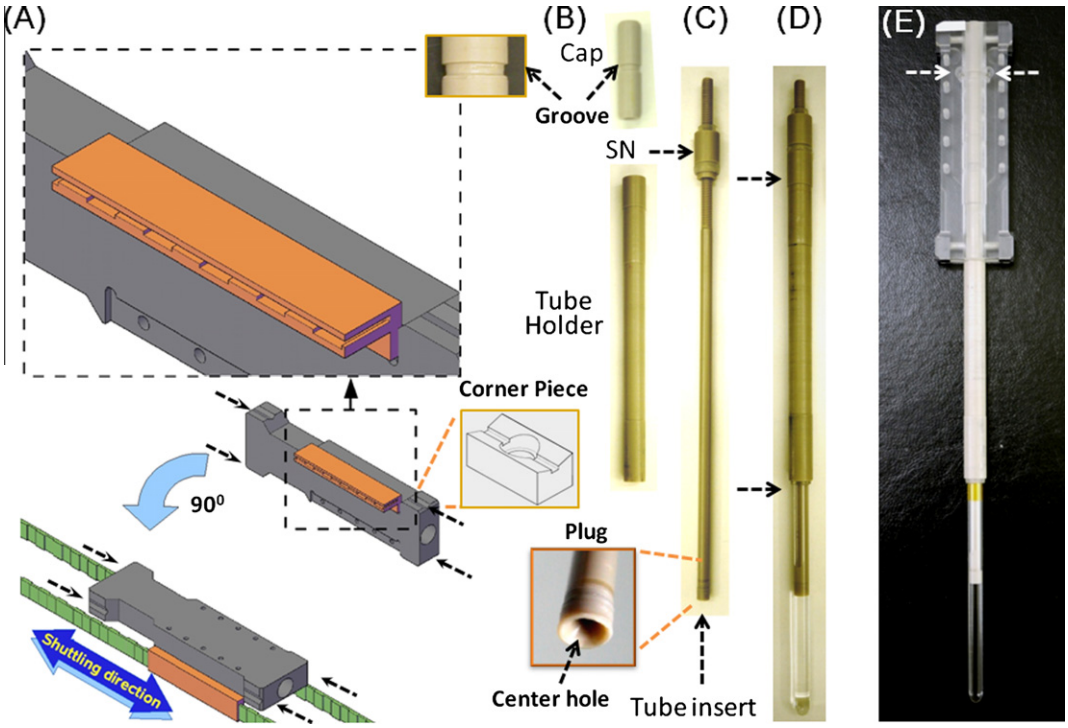

Fig. 3. (A) A schematics showing the shuttle/timing belt coupling mechanism. The enlarged F-shaped coupler (colored orange) with 10 teeth is shown on the top. The shuttle with timing belt attached is shown on the bottom. The four arrows indicate the positions of the four corner pieces with V-shaped grooves. The insert in the middle shows the corner piece design. (B) Photograph of the cap (top) and tube holder (bottom). In the middle of the cap is a 3 mm wide constriction groove (inset) of 6 mm outer diameter for restricting the movement of the cap by two screws. (C) The NMR tube insert. An expanded view of the bottom plug section is shown on the bottom. The screw nut (SN) is screwed on the threaded rod and can be moved up or down by turning. (D) Photograph of the assembled NMR sample assembly. Two silicon O-rings are placed at the positions indicated by the two arrows. (E) The completely assembled shuttle/sample assembly. The two arrows indicated the two screws employed for restricting the movement of the cap.

the power supply are housed in an outside case. The optical sensor circuitry and digital control circuitry are wired on a circuit board mounted on top of the magnet and interfaced to the spectrometer PC via a USB connection. During operation the pulse program sends out pulses to the control board to trigger the operation of the motor as specified by a program stored in a microprocessor on the motor driver module. The "start" pulse received from the pulse program also initiates a timer and records the detecting times of each optical sensor signal for monitoring the shuttle positions. The time–position information also serves as a safety check and detection of an abnormal time–position data triggers a "stop" signal to suspend the shuttling operation.

3. Results and discussion

3.1. Sample preparation and loading

The 5 mm NMR tube preloaded with sample (0.25–0.5 ml) was first placed inside the tube holder with the two ends secured with two silicon O-rings to prevent the NMR tube from slipping along the holder. With the sample in an upright position the tube insert was then gradually pushed into the NMR tube until a small volume of sample flowed out of the side hole of the insert to ensure no air bubble in the sample chamber. The sample position was further fine tuned by adjusting the positions of the O-ring and the screw nut such that the bottom of the screw nut snaps onto the tube holder snugly (Fig. 3D). The completely assembled sample was then inserted into the sample-holding hole at the center of the shuttle. Subsequently, the sample assembly was covered with a cap whose position was secured on the shuttle with two screws protruding into the constriction groove of the cap (indicated by the two arrows in Fig. 3E) to restrict the upward motion of the sample assembly with respect to the shuttle. The completely assembled shuttle/sample assembly is shown in Fig. 3E. For an experienced user this sample assembly process takes less than 10 min to complete and the sample is secured in the shuttle with no slipping for many experiments in the last 12 months.

3.2. The shuttling speed

The shuttle trajectory can be programmed in various desired modes by controlling the servomotor with machine-language programs encoded in a microprocessor on the motor driver module. We programmed the driver to run the servomotor in constant acceleration mode for the first half of the shuttling process and constant deceleration mode for the remainder of the trip. This operation gives the shortest traveling time at the smallest acceleration. In this mode, two parameters are used to specify the trajectory of a particular experiment, i.e. the angular acceleration/deceleration rate of the motor and the traveling distance.

The linear acceleration of the shuttle is determined by the motor angular acceleration and the diameter of the large pulley. The maximal angular acceleration specified for the current motor is 1000 rps^2. Thus, for a pulley with 120 mm diameter the allowed maximum acceleration is 377 m/s^2, or 38.5G, where G is the gravitational acceleration. Ideally, at this acceleration the shuttle can travel to the top of the magnet at 90 cm above in 98 ms. In practice, the highest angular acceleration we have achieved was 800 rps^2, likely limited by the torque the motor can deliver. We have not tried a higher power motor for achieving higher shuttling speed. Fig. 4 shows the field plot (Fig. 4A) and the trajectories (Fig. 4B) of a typical run at 700 rps^2 angular acceleration. The time courses fit well to the theoretical curves for both rising and lowering periods, suggesting that indeed the sample is moving at the specified

constant acceleration–deceleration rates. At this acceleration it took ~117 ms to shuttle the sample from the center of the magnet to the top. The data are fully reproducible.

3.3. System stability and accuracy

The servomotor has a feedback mechanism for reducing overshoot and position instability. This is achieved through optimizing the proportional–integral-derivative (PID) controller. When the PID was optimized in the programmed constant acceleration/deceleration mode our shuttle device moved and stopped smoothly and stabilized quickly without noticeable instability. We found that the field could be locked in 13 ms after the sample had returned to the center of the magnet and data acquisition could begin thereafter. The dead time is independent of the travel distance. For comparison, the dead time for field locking of a pneumatic shuttle device we also built was ~150 ms. This effectively added an additional 150 ms in shuttling time. In addition, under the programmed trajectory the samples started and stopped smoothly and were subjected to much less stress, thereby reducing the chance of bubble formation that causes sample denaturation.

The capability of the shuttle to return to the same position accurately is an important issue for long term stability. The servomotor has a resolution of 0.18°/step, or 0.188 mm/step in the accuracy of the shuttle vertical position for our setup. This number was roughly confirmed by the change in lock level. In our system when the sample position was deliberately misplaced by 1 mm the lock level changes by 0.04 divisions. During the shuttling period the lock was put on hold and was reactivated 13 ms after the sample had returned to the center of the magnet. In this mode of operation the lock level fluctuation was insignificant. Fig. 5A showed two 1D ^{13}C spectra of (3,3,3-d_3)-alanine obtained with (Fig. 5A) or without (Fig. 5B) shuttling to a field of 2.93 T. The time between the start of shuttling and the beginning of signal detection was kept at 1.0 s in both cases. The signal-to-noise ratios of the two spectra were indistinguishable. Repeated shuttling appeared to have little effect on the shimming, as demonstrated by the stable lock level measured over 35 h for a total of 25,000 trips. This indicated that the device was able to return the sample to the precise location at the center of the magnet with long term stability.

3.4. Field-dependent ^{13}C–T_1 relaxation of (3,3,3-d)-alanine carboxyl carbon

To demonstrate the utility of the field cycling device we measured the ^{13}C–T_1 of the carboxyl ^{13}C nucleus of (3,3,3-d)-alanine at fields from 0.04 to 14.1 T. The relaxation rates were measured in D_2O to eliminate the possible dipolar contribution from solvent and amide protons. Longitudinal relaxation rates were measured by the inversion-recovery method of the following pulse sequence: 180° – shuttling up – τ – shuttling down – 90° – recycle delay, where τ is the relaxation delay at the desired low field and the recycle delay time is set at >5T_1. The ^{13}C–T_1 of alanine carboxyl carbon is dominated by both ^1H–^{13}C dipolar interaction and ^{13}C chemical shift interaction (CSA) as described by the following equations [2,34]:

$$R_1 = R_1(\text{dipolar}) + R_1(\text{CSA}) \tag{1}$$

$$R_1(\text{dipolar}) = \left(\frac{\mu_0}{4\pi}\right)\frac{h^2\gamma_H^2\gamma_C^2}{2r_{CH}^6}[0.1J_{DD}(\omega_H-\omega_C)+0.3J_{DD}(\omega_C)+0.6J_{DD}(\omega_H+\omega_C)] \tag{2}$$

$$R_1(\text{CSA}) = \left(\frac{1}{15}\right)\sigma^2\left(1+\frac{\eta^2}{3}\right)\cdot(\gamma_C B)^2\cdot J_{CSA}(\omega) \tag{3}$$

Here B is the magnetic field strength, $\hbar$ is Plank's constant divided by 2π, μ_0 is permittivity of free space ω_i is the angular Larmor frequency for spin I, γ_i is the gyromagnetic ratios for spin i, r_{CH} is the ^{13}C–^1H distance and $J_{DD}(\omega) = 2\tau/(1+\omega^2\tau^2)$ is the spectral density function for the dipolar contribution. σ and η are the magnitude and the asymmetry parameter of the CSA, respectively.

The CSA contribution to the longitudinal relaxation can be separated into two terms, $J_{CSA}(\omega) = S_C^2\frac{2\tau}{(1+\omega^2\tau^2)} + (1-S_C^2)\frac{2\tau_f}{1+\omega^2\tau_f^2}$. The first term was previously referred to as low-field CSA (CSA_L), which characterizes the overall tumbling of the macromolecule. The second term was referred to as the high-field CSA (CSA_H) contribution describing the fast internal motion [34,35]. The relative contribution of different terms can be extracted from fitting of the field-dependent R_1 curve. However, for small molecule such as alanine which tumbles very rapidly in aqueous solution the low-field contribution dominates and the second high-field term can be ignored.

Fig. 5C shows the experimental field-dependent $R_1(\omega)$ profile and the simulated results of the contribution from low-field CSA_L (green solid line), high-field CSA_H (green dashed line) and dipolar (blue solid line) contributions to the relaxation. In the fitting three parameters were allowed to vary, namely the rotational correlation time, τ; the distance between dipolar pairs, r; and $\sigma^2(1+\eta^2/3)$. The chemical shift tensor, σ, and the asymmetry parameter of the chemical shift tensor, η, were lumped together in a single term. For the (3,3,3-d_3)-alanine the only dipolar contribution is that from the H^α at 2.1 Å away, thus the dipolar contribution can be described by a two-spin treatment. The simulated rotational correlation time is τ = 57 ps, which is reasonable for the small amino acid.

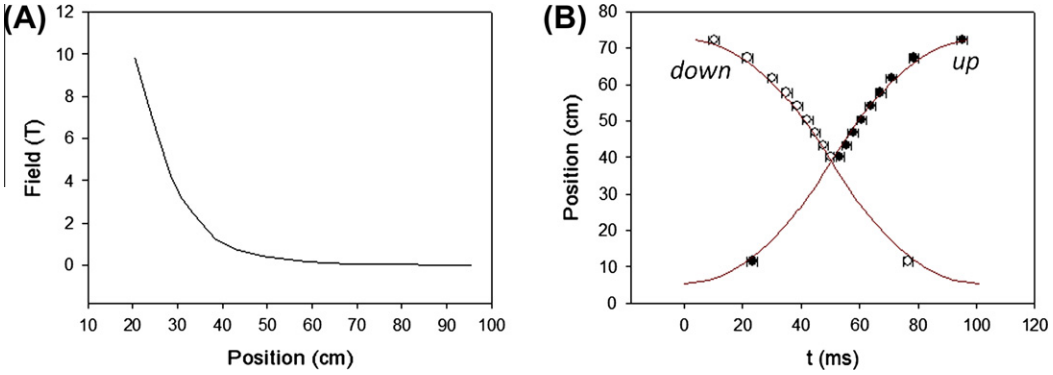

Fig. 4. (A) Field plot of the spectrometer magnet. (B) The trajectory of the shuttle during the rising (solid dots) and lowering (open circles) period. The servomotor operates at a constant acceleration mode for the first half of the trip and constant deceleration mode during the second half of the trip. The angular acceleration/deceleration was set at 700 rps^2. The positions were detected with optical sensors attached at various positions of the rail, as indicated. The center of the magnet is defined as the "0" displacement. (For interpretation of color in this figure, the reader is referred to the web version of this article.) The solid lines are the theoretical trajectories.

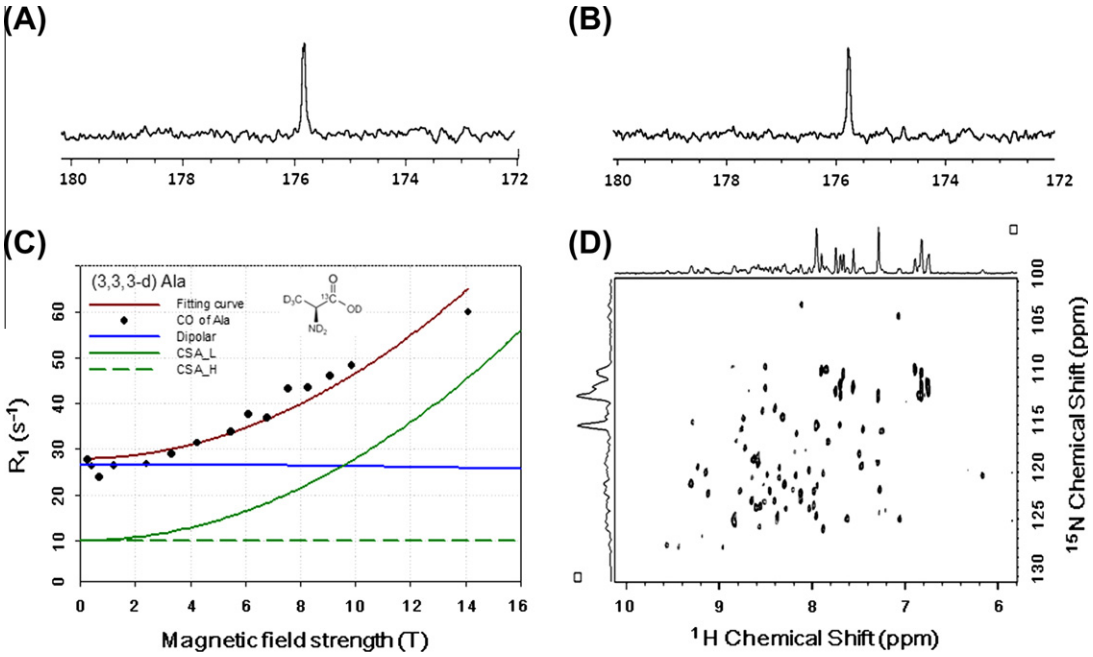

Fig. 5. (A) A 1D ^{13}C spectrum of (3,3,3-d_3)-alanine (50 mg/ml in 50 mM potassium phosphate buffer, pH 6.0) obtained after shuttling to 2.93 T and back at 14.1 T for detection. Each spectrum is the averaging of eight scans. The run-trip shuttling time was 130 ms and the relaxation time was 857 ms and the signal was detected at 1 s after start of the shuttling process. (B) ^{13}C spectrum (3,3,3-d_3)-alanine obtained with 1.0 s relaxation delay at 14.1 s without shuttling to low field. (C). Field-dependent ^{13}C relaxation rates (R_1) of (3,3,3-d_3) alanine (sample condition same as in A and B). The solid red line is fitted to the data, taking into account of the contributions from dipolar interaction (blue solid line) and low-field CSA (green solid line). Contribution of the high-field CSA (green dash line) is negligible as expected. (D) A 2D ^{15}N-HSQC spectrum of (u-^{13}C) ubiquitin (1.0 mM in 50 mM potassium phosphate buffer, pH 6.0 in 10% D_2O). Data were obtained at room temperature. The ^{15}N-HSQC spectrum is selected from a series of field-dependent ^{15}N–T_1 experiment with relaxation delay of 153 ms at 3.77 T and detection at 14.1 T. The experimental conditions are: 2048 points in t1 dimension and 128 points in t2 dimension with recycling delay of 5 s and 2 scan averaging. It took 67 ms to shuttle the sample to 3.77 T. The 1D projection of ^{15}N and ^{1}H dimensions were shown to show the spectral quality.

The simulated ^{13}CO–H^{α} distance of 2.15 Å is also in agreement with the known distance of 2.1 Å. The simulated value of $\sigma^2(1+\eta^2/3)$ the carbonyl carbon was 11,700 ppm^2, which compares favorably with the value of 9414 ppm^2 determined from solid state experiment [36,37].

3.5. Field-dependent amide ^{15}N–T_1 of proteins

As a more stringent test of the system stability we measured the backbone amide ^{15}N–T_1 of (u-^{15}N)-ubiquitin at fields ranging from 3.77 T to 14.1 T and detection at 14.1 T. The run-trip shuttling time between these two fields was 120 ms. The data were acquired at room temperature using the pulse sequence developed by Kay et al. on a standard 5 mm QXI probe [13]. A typical 2D ^{15}N-HSQC with 153 ms relaxation delay at 3.77 T is shown in Fig. 5D. At low field the ^{15}N–T_1 of the amide nitrogen is dominated by ^{15}N–^{1}H dipolar coupling. For ubiquitin the rotational correlation time at room temperature is ~4 ns [38] and the ^{15}N–T_1 at 3.77 T is ~100 ms (Chou and Huang, unpublished observation). The quality of the spectrum attests to the suitability of the device for performing multi-dimensional NMR experiments of spin with T_1 as low as 100 ms in H_2O. However, it will be rather challenging to measure ^{15}N–T_1 much below 4 T since ^{15}N–T_1 decreases rapidly at lower field. On the other hand, it should be more favorable to measure the carbonyl ^{13}C–T_1 at low fields for deuterated samples since the dipolar effect on carbonyl ^{13}C is less severe.

4. Conclusions

We report the design and performance of a compact high-speed mechanical sample shuttling system. In comparison to an earlier pneumatic shuttling device we built, based on Redfield's design, the mechanical device is more compact and easier to handle. More importantly, the mechanical system is more stable and the greatly reduced dead time due to fast sample damping upon returning to the high field position making it suitable for the shuttle device to measuring T_1 relaxation time shorter than 100 ms. A larger diameter pulley coupled with a motor that generates higher torque could possibly reduce the shuttling time further. The lowest field that can be achieved in our system is the stray field on the top of the magnet, which is ~200 Gauss. Measurement of the relaxation rate at even lower field can be achieved by installing a Helmholtz coil on top of the magnet, as was done by Ivanov and Redfield [39].

In spite of many exciting results published in recent years, especially those by Redfield and coworkers regarding the structure and dynamics of lipid membrane and protein systems (for a review see Redfield 2011) [29,40–43], the field-cycling technique is still not popular among high resolution biomacromolecular researchers, presumably due to limited access to the field cycling device. Here we report a design that is not too difficult to make, easy to install, convenient to use, and robust in operation. Our system should be of interests to those who are interested in exploring many more exciting applications that require a fast and reliable sample shuttling device. A concern of strong magnetic field gradient due to inhomogeneity of the fringe field may not be as serious for most applications, as discussed by Redfield [25].

Acknowledgments

We are grateful to Prof. A.G. Redfield for his encouragement and for providing us with details of his pneumatic design before publication. We thank the staffs in the Academia Sinica Machine Shop, Taiwan, especially Mr. Cherng-Yin Lin and Ta-Horng Liao, for the production of high precision hardware, Mr. Fong-Ku Shi and

Mr. Jimmy Wu of Rezwave Technology Inc., Taiwan for technical assistances. This work is supported by a Grants NSC99-3112-B-001-027 from The National Science Council and NHRI-EX99-9933B1 from the National Health Research Institute of the Republic of China to THH. The NMR experiments were carried out with NMR spectrometers of the High-Field Nuclear Magnetic Resonance Center (HFNMRC) supported by National Research Program for Genomic Medicine, The National Science Council of the Republic of China.

References

[1] N. Bloembergen, E.M. Purcell, R.V. Pound, Relaxation effects in nuclear magnetic resonance absorption, Phys. Rev. 73 (1948) 679–712.
[2] A. Abragam, The Principles of Nuclear Magnetism, Clarendon Press, Oxford, UK, 1961.
[3] R.V. Pound, Nuclear spin relaxation time in a single crystal of LiF, Phys. Rev. 81 (1951) 156.
[4] A. Abragam, R.V. Pound, Influence of electric and magnetic fields on angular correlations, Phys. Rev. 92 (1953) 943.
[5] P.N. Argyres, P.L. Kelley, Theory of spin resonance and relaxation, Phys. Rev. 134 (1964) A98.
[6] F. Bloch, Line-narrowing by macroscopic motion, Phys. Rev. 94 (1954) 496.
[7] F. Bloch, Generalized theory of relaxation, Phys. Rev. 105 (1957) 1206.
[8] A.G. Palmer, Probing molecular motion by NMR, Curr. Opin. Struct. Biol. 7 (1997) 732–737.
[9] K. Henzler-Wildman, D. Kern, Dynamic personalities of proteins, Nature 450 (2007) 964–972.
[10] D.D. Boehr, H.J. Dyson, P.E. Wright, An NMR perspective on enzyme dynamics, Chem. Rev. 106 (2006) 3055–3079.
[11] G. Lipari, A. Szabo, Model-free approach to the interpretation of nuclear magnetic resonance relaxation in macromolecules. I. Theory and range of validity, J. Am. Chem. Soc. 104 (1982) 4546–4559.
[12] G. Lipari, A. Szabo, Model-free approach to the interpretation of nuclear magnetic resonance relaxation in macromolecules. II. Analysis of experimental results, J. Am. Chem. Soc. 104 (1982) 4559–4570.
[13] L.E. Kay, D.A. Torchia, A. Bax, Backbone dynamics of proteins as studied by nitrogen-15 inverse detected heteronuclear NMR spectroscopy: application to staphylococcal nuclease, Biochemistry (Wash.) 28 (1989) 8972–8979.
[14] B. Halle, V.P. Denisov, Magnetic relaxation dispersion studies of biomolecular solutions, Methods Enzymol. 338 (Part A) (2001) 178–201.
[15] R. Kimmich, W. Nusser, T. Gneiting, Molecular theory for nuclear magnetic-relaxation in protein solutions and tissue – surface-diffusion and free-volume analogy, Colloid Surf. 45 (1990) 283–302.
[16] W. Nusser, R. Kimmich, Protein backbone fluctuations and NMR field-cycling relaxation spectroscopy, J. Phys. Chem. 94 (1990) 5637–5639.
[17] R. Kimmich, E. Anoardo, Field-cycling NMR relaxometry, Prog. Nucl. Magn. Reson. Spectrosc. 44 (2004) 257–320.
[18] A.G. Redfield, Field cycling NMR applied to macromolecular structure and dynamics, in: B.D.N. Rao, M.D. Kemple (Eds.), NMR as a Structural Tool for Macromolecules, Plenum Press, New York, 1996, pp. 123–132.
[19] F. Noack, NMR field-cycling spectroscopy – principles and applications, Prog. Nucl. Magn. Reson. Spectrosc. 18 (1986) 171–276.
[20] S.H. Koenig, The dynamics of water in biological systems, in: D.M. Grant, R.K. Harris (Eds.), Encyclopedia of NMR, John Wiley, New York, 1995, pp. 1817–1830.
[21] E.P. Sunde, B. Halle, Slow internal protein dynamics from water 1H magnetic relaxation dispersion, J. Am. Chem. Soc. 131 (2009) 18214–18215.
[22] C. Job, J. Zajicek, M.F. Brown, Fast field-cycling nuclear magnetic resonance spectrometer, Rev. Sci. Instrum. 67 (1996) 2113–2122.
[23] R. Kimmich, NMR: Tomography, Diffusometry, Relaxometry, Springer-Verlag, Heidelberg, 1997.
[24] F. Noack, Field cycling experiments, in: Encyclopedia of Magnetic Resonance, John Wiley & Sons, New York, 2007, pp. 1980–1990.
[25] A.G. Redfield, Shuttling device for high-resolution measurements of relaxation and related phenomena in solution at low field, using a shared commercial 500 MHz NMR instrument, Magn. Reson. Chem. 41 (2003) 753–768.
[26] S. Wagner, T.R. Dinesen, T. Rayner, R.G. Bryant, High-resolution magnetic relaxation dispersion measurements of solute spin probes using a dual-magnet system, J. Magn. Reson. 140 (1999) 172–178.
[27] K. Victor, V. Kavolius, R.G. Bryant, Magnetic relaxation dispersion probe, J. Magn. Reson. 171 (2004) 253–257.
[28] D.J. Kerwood, P.H. Bolton, A sample-shuttling device suitable for two-dimensional low-field NMR, J. Magn. Reson. 75 (1987) 142–146.
[29] A.G. Redfield, High-resolution NMR field-cycling device for full-range relaxation and structural studies of biopolymers on a shared commercial instrument, J. Biomol. NMR, in press.
[30] S. Grosse, F. Gubaydullin, H. Scheelken, H.-M. Vieth, A.V. Yurkovskaya, Field cycling by fast NMR probe transfer: design and application in field-dependent CIDNP experiments, Appl. Magn. Reson. 17 (1999) 211–225.
[31] S. Grosse, A.V. Yurkovskaya, J. Lopez, H.-M. Vieth, Field dependence of chemically induced dynamic nuclear polarization (CIDNP) in the photoreaction of N-acetyl Histidine with 2,2′-dipyridyl in aqueous solution, J. Phys. Chem. A 105 (2001) 6311–6319.
[32] H.M. Vieth, S. Grosse, F. Gubaydullin, H. Scheelken, A.V. Yurkovskaya, Field cycling by fast NMR probe transfer: design and application in field-dependent CIDNP experiments, Appl. Magn. Reson. 17 (1999) 211–225.
[33] H. Stork, M. Ditter, H. Plößer, A.F. Privalov, F. Fujara, High temperature mechanical field-cycling setup, J. Magn. Reson. 192 (2008) 173–176.
[34] M.F. Roberts, Q. Cui, C.J. Turner, D.A. Case, A.G. Redfield, High-resolution field-cycling NMR studies of a DNA octamer as a probe of phosphodiester dynamics and comparison with computer simulation, Biochemistry (Wash.) 43 (2004) 3637–3650.
[35] M.F. Roberts, A.G. Redfield, Phospholipid bilayer surface configuration probed quantitatively by (31)P field-cycling NMR, Proc. Natl. Acad. Sci. USA 101 (2004) 17066–17071.
[36] C. Ye, R. Fu, J. Hu, L. Hou, S. Ding, Carbon-13 chemical shift anisotropies of solid amino acids, Magn. Reson. Chem. 31 (1993) 699–704.
[37] Z. Gu, R. Zambrano, A. McDermott, Hydrogen bonding of carboxyl groups in solid-state amino acids and peptides: comparison of carbon chemical shielding, infrared frequencies, and structures, J. Am. Chem. Soc. 116 (1994) 6368–6372.
[38] S.L. Chang, N. Tjandra, Temperature dependence of protein backbone motion from carbonyl C-13 and amide N-15 NMR relaxation, J. Magn. Reson. 174 (2005) 43–53.
[39] D. Ivanov, A.G. Redfield, Field-cycling method with central transition readout for pure quadrupole resonance detection in dilute systems, J. Magn. Reson. 166 (2004) 19–27.
[40] M.F. Roberts, A.G. Redfield, High-resolution P-31 field cycling NMR as a probe of phospholipid dynamics, J. Am. Chem. Soc. 126 (2004) 13765–13777.
[41] M.F. Roberts, A.G. Redfield, Phospholipid bilayer surface configuration probed quantitatively by P-31 field-cycling NMR, Proc. Natl. Acad. Sci. USA 101 (2004) 17066–17071.
[42] M.W. Clarkson, M. Lei, E.Z. Eisenmesser, W. Labeikovsky, A. Redfield, D. Kern, Mesodynamics in the SARS nucleocapsid measured by NMR field cycling, J. Biomol. NMR 45 (2009) 217–225.
[43] M. Pu, A. Orr, A.G. Redfield, M.F. Roberts, Defining specific lipid binding sites for a peripheral membrane protein in situ using subtesla field-cycling NMR, J. Biol. Chem. 285 (2010) 26916–26922.